Transient dendritic cell activation diversifies the T cell response to acute infection

Matthew Spitzer (Matthew.Spitzer@ucsf.edu)
University of California, San Francisco https://orcid.org/0000-0002-5291-3819
Kamir Hiam-Galvez
UCSF https://orcid.org/0000-0002-1956-0257
Rachel DeBarge
UCSF
Caleb Lareau
Stanford University School of Medicine https://orcid.org/0000-0003-4179-4807
Nam Woo Cho
UCSF
Jacqueline Yee
UCSF
Trine Line Okholm
UCSF https://orcid.org/0000-0002-2779-4029

Article

Keywords: T cell priming, Listeria monocytogenes, conventional type 1 dendritic cells

Posted Date: November 1st, 2021

DOI: https://doi.org/10.21203/rs.3.rs-1013987/v1

Title: Transient dendritic cell activation diversifies the T cell response to acute infection

Authors: Kamir J. Hiam-Galvez[1-3], Rachel DeBarge[1,2], Caleb A. Lareau[3], Nam Woo Cho [2,4], Jacqueline L. Yee[1,2], Trine Line H. Okholm[2], Matthew H. Spitzer[1,2]*

Affiliations:

[1]Graduate Program in Biomedical Sciences, University of California, San Francisco; San Francisco, CA, USA

[2]Departments of Otolaryngology and Microbiology & Immunology, Helen Diller Family Comprehensive Cancer Center, Parker Institute for Cancer Immunotherapy, Chan Zuckerberg Biohub, University of California, San Francisco; San Francisco, CA, USA

[3]Department of Pathology, Stanford University; Stanford, CA, USA

[4]Department of Radiation Oncology, University of California San Francisco; San Francisco, CA, USA

*Corresponding author. Email: matthew.spitzer@ucsf.edu

Abstract: The precise timing of T cell priming during infection remains unclear. Here, we mapped the cellular dynamics of all immune lineages during acute infection with *Listeria monocytogenes* (*Lm*). We identified highly transient activation of conventional type 1 dendritic cells (cDC1s) two days post-infection that functions as a critical time window for priming effector CD8 T cells. Regulation of this transient state was mediated by cDC1-extrinsic IFNγ provided by lymphocytes. Furthermore, antigen-specific T cells that are primed by cDC1s even shortly after this window of peak activation acquire only memory T cell fates. This temporal regulation of fate is recapitulated by cDC1s *ex vivo*, demonstrating that shifts in activation state of a single antigen presenting cell subset over time regulates CD8 T cell fates. These results uncover a novel mechanism for temporal regulation of CD8 T cell differentiation during a dynamic immune response to acute infection.

One of the most important cellular interactions mediating protective adaptive immune responses is the priming of CD8 T cells by cDC1s. Upon recognition of cognate antigen presented on Major Histocompatibility Complex class I (MHCI) by cDC1s, CD8 T cells rapidly divide and differentiate into multiple mature effector populations [1]. Early decisions in T cell fate lead to the acquisition of functionally distinct differentiation states including memory and cytotoxic short-lived effector cell (SLEC) phenotypes[1]. While SLECs carry out critical effector functions to clear an infection, such as direct cellular cytotoxicity of infected cells and production of inflammatory cytokines, long-lived memory cells a critical component of immunological memory, enabling rapid recall responses upon secondary infection[2].

Intriguingly, single cells are committed to specific fates very early after priming by cDC1s[3,4]. However, most prior studies have focused on CD8 T cell-intrinsic mechanisms of fate determination. A variety of key transcription factors and transcriptional repressors regulate the differentiation toward effector or memory cell fates, including T-bet, eomesodermin, BLIMP1/BCL-6, and ID2/ID3 among others[5]. In addition, CD8 T cells acquire different metabolic programs that in turn regulate differentiation[6]. In comparison, less work has focused on cell-extrinsic regulation of CD8 T cell differentiation.

DCs are highly responsive to environmental stimuli while also possessing several mechanisms to prevent their hyperactivation. Therefore, we wondered whether regulation of cDC1 activation over time might contribute to the diversification of CD8 T cell fates to balance effector and memory T cell differentiation. We sought to map cDC1 activation throughout infection, identify regulatory mechanisms of cDC1 activation, and define the phenotypic landscape of T cells primed at different stages of cDC1 activation. These experiments yield results with important implications for how cDC1s induce the differentiation of diverse CD8 T cell fates during natural immune responses and how this might be therapeutically manipulated in different contexts.

Immune Landscapes During Acute Infection

To map the complete immune response to acute infection with *Lm* expressing the model antigen ovalbumin (*LmOVA*), wild type C57BL/6 mice were infected intravenously, and spleen tissue was harvested every day for the first 9 days of infection. To quantify the frequencies and activation states of immune cells, we used mass cytometry to profile over 4 million single cells using a panel of 41 antibodies designed to identify all mature immune lineages with the addition of several markers that specify activated states of antigen presenting cells and T cells (Supplementary Fig. 1, Supplementary Table 1)[7,8]. We identified distinct cell states through unsupervised clustering and observed highly transient immune landscapes throughout different stages of infection (Fig. 1a-d, Supplementary Fig. 2a). We saw modest compositional changes 1 day post infection (DPI) followed by more substantial innate immune activation from 2-5 DPI and the emergence of activated T cells from 6-9 DPI (Fig. 1a-d). We found equivalent changes in immune landscapes when assessing manually gated immune cell populations or unsupervised clusters of immune cells (Supplementary Fig. 2b-c).

Quantifying compositional changes by Aitchison distance, we found that the global composition of immune cells remained highly distinct from uninfected animals throughout infection, and substantial changes were evident between each subsequent day, underscoring the dynamicity of the response (Fig. 1e). Compositional changes between consecutive days began to decrease at 6 DPI with the smallest changes seen between 8-9 DPI (Fig. 1e), consistent with the resolution of infection. Activated CD8 T cells, a critical adaptive immune cell type required for clearance of *Lm* infection[9,10], began to emerge in significant frequencies at 5 DPI followed by the acquisition

of terminally differentiated fates (Fig. 1f, Supplementary Fig. 2d). This suggests that key T cell priming events occur early during infection.

Dendritic Cell Activation During Acute Infection

Given the dynamic changes to innate immune populations early in infection, we next sought to assess the activation dynamics of cDC1s, the principal cell type that primes CD8 T cells in *Lm*[11]. Consistent with previous findings, we found that *Batf3*$^{-/-}$ mice lacking cDC1s exhibited deficient CD8 T cell responses to *Lm* infection (Fig. 2a). To further assess the activation state of cDC1s over time, we calculated a composite activation score based on the expression of key molecules associated with activation. We found that cDC1 activation reached a transient peak at 2 DPI that was significantly higher than the previous or subsequent day (Fig. 2b-c). Variance in cDC1 activation score was also highest at 2 DPI, suggesting that cDC1s from this timepoint exhibit the widest range of activation states that an individual T cell could interact with (Fig. 2b). We also found that cDC1s presenting SIINFEKL:H2-K^{b} complexes (an immunodominant OVA antigen in the context of MHC class I) on the cell surface were most abundant at 2 DPI as measured by flow cytometry (Fig. 2d, Supplementary Fig. 3). The limit of detection for the antibody clone 25-D1.16 that recognizes SIINFEKL:H2-K^{b} is greater than that for CD8 T cell activation[12]; thus, these data indicate that cDC1s at 2 DPI have the highest levels of cell surface SIINFEKL:H2-K^{b} but do not suggest that SIINFEKL:H2-K^{b} complexes are absent at other timepoints. We further examined cDC1 activation in mouse cytomegalovirus (MCMV) infection and found that cDC1s were similarly most activated at 2 DPI in a highly transient manner (Fig. 2e-f).

To map cDC1 activation more comprehensively, we utilized mass cytometry with an extended panel of activation molecules. We visualized cDC1s using PHATE dimensionality reduction [13] along with Slingshot lineage reconstruction[14] (Fig. 3a-c), which revealed a highly coordinated cDC1 activation trajectory. We calculated Pseudotime values for individual cDC1s over this activation trajectory, which was characterized by increasing expression of all activation markers from minimum to maximum Pseudotime (Fig. 3a-c). Activation and costimulatory molecules had distinct patterns of upregulation; for instance, CD86 expression steadily increased throughout the trajectory, while CD70 expression only increased in cells at the maximum end of the Pseudotime trajectory (Fig. 3a-c). We found similar gradients of cDC1 activation from MCMV infected mice (Fig. 3d-f). cDC1s from MCMV infection showed very similar increases in key markers CD86, CD80, CD83, and PDL1 expression when compared to cDC1s from *Lm* infection. In contrast to *Lm* infection, CD70+ cDC1s were primarily detected at an intermediate activation state in MCMV infection. Together, these data reveal a unique cDC1 activation state transiently arises only at 2 DPI, which represents the most highly activated cDC1 state during acute infection.

Cell-Extrinsic Regulation of Transient Dendritic Cell Activation

To identify the mechanisms by which peak cDC1 activation is regulated at 2 DPI, we first quantified cytokines from spleen tissue homogenate during early infection. We found that samples from 2 and 3 DPI had markedly different cytokine landscapes from each other and from uninfected and 1 DPI samples (Fig. 4a, Supplementary Fig. 4a). Specifically, IFNγ levels peaked at 2 DPI, and IFNγ was the primary cytokine driving differences in the cytokine landscape on 2 DPI (Fig. 4b). A previous study found that IFNγ signaling mediates IL-12 production by DCs[15], supporting a role for this pathway in promoting DC activation. The STAT1 signaling pathway is prototypically activated by IFNγ[16]. Therefore, we quantified levels of phosphorylated STAT1

(pSTAT1) at 2 DPI in cDC1s. Indeed, cDC1s had elevated levels of pSTAT1, consistent with IFNγ signaling acting directly on cDC1s (Fig. 4c).

To assess whether cell-intrinsic recognition of *Lm* by pattern recognition receptors activated STAT1 signaling, we incubated cDC1s with heat killed *Lm* (HKLM) *in vitro* and quantified cell signaling responses. While we observed signaling through IkBa, pERK, and pP38 (Supplementary Fig. 4b), we found no change in pSTAT1 (Fig. 4c). These results suggest that pSTAT1 signaling in cDC1s at 2 DPI *in vivo* is not due to direct recognition of *Lm* but may instead result from cell-extrinsic IFNγ. To validate the observed kinetics of IFNγ production, and to identify the cellular source of IFNγ, we utilized an IFNγ GFP reporter mouse[17] and found that splenic GFP+ IFNγ-producing cells are undetectable at 1 DPI but prominent at 2 DPI (Fig. 4d, Supplementary Fig. 4c). We further found that the majority of these IFNγ producing cells at 2 DPI were T and NK cells (Fig. 4e, Supplementary Fig. 4d-e). We then depleted NK cells or Thy1+ lymphocytes and observed that only Thy1 depletion significantly decreased IFNγ levels in the spleen at 2 DPI (Fig. 4f, Supplementary Fig. 4f). Both depletion of Thy1+ cells and antibody neutralization of IFNγ significantly decreased splenic cDC1 activation at 2 DPI (Fig. 4g-h). Together these data suggest that peak cDC1 activation is dependent on a transient burst of cell-extrinsic IFNγ produced by lymphocytes on 2 DPI.

Transient Dendritic Cell Activation Regulates T Cell Fate

Next, we sought to understand the functional consequences of transient cDC1 activation. We reasoned that all T cells capable of recognizing a specific antigen during acute infection are dispersed throughout the organism, and that priming occurs in specific secondary lymphoid organs (SLO) where antigens are present. Using relevant parameters from the literature, we developed a computational model of T cells encountering SLOs as a function of time post-infection utilizing a multinomial sampling procedure (Methods). Our simulations showed that, throughout an acute infection, naïve antigen specific T cells continually enter priming SLOs over time (Fig. 5a), even after accounting for inflammation induced recirculation which increases the rate of T cell trafficking[18,19]. Thus, a meaningful fraction of naïve T cells will likely arrive to the site of priming after 2 DPI, when peak cDC1 activation occurs (Fig. 5a). Based on our experimental observations, these late arriving antigen specific cells will encounter a dramatically shifting landscape of antigen presenting cells, and specifically, different activation states of cDC1s. Consistent with our model, we found that inhibiting lymphocyte trafficking using FTY720 reduced the number of splenic CD8 T cells on 3 DPI that exhibited evidence of recent TCR signaling, using a reporter for Nur77 (Supplementary Fig. 5a).

To experimentally test the effects of transient cDC1 activation, we adoptively transferred TCR transgenic OT1 CD8 T cells on each of 0-4 DPI with *Lm*-OVA and assessed OT1 fate in the spleen 7 days after transfer (Fig. 5b). In this model system, cells transferred in at 3 and 4 DPI miss the transient cDC1 activation peak on 2 DPI. We found that the magnitude of T cell expansion was significantly decreased over time, as measured by the total numbers of splenic OT1 CD8 T cells (Fig. 5c). We also found that OT1 cell fate shifted from primarily KLRG1+CD62L- short-lived effector cell (SLEC) fate to KLRG1-CD62L+ central memory fate as a function of time, and SLEC differentiation was entirely lost after 2 DPI (Fig. 5d-f). We delved deeper into the phenotypes of CD8 T cells transferred on 0 versus 3 DPI using an extended antibody panel and found that cells transferred at these timepoints differentiated into unique cell states (Fig. 5g-h). The memory phenotype exhibited by 3 DPI cells was uniquely characterized by expression of CD90, CD127, TCF1 and CD62L (Fig. 5h). The effector phenotype exhibited by 0 DPI cells was instead characterized by expression of PD1, Ki67,

CD25, Granzyme B, KLRG1, and CD11c (Fig. 5h). We found identical results utilizing low affinity OT3 TCR transgenic CD8 T cells[20] with *Lm*-OVA infection (Fig. 5i-j, Supplementary Fig. 5b) as well as with adoptive transfer of polyclonal T cells in the context of MCMV infection (Fig. 5k-l, Supplementary Fig. 5c). This suggests that transient cDC1 activation regulates the balance between SLEC and memory CD8 T cell differentiation regardless of TCR affinity and across infection contexts. We confirmed that OT1 T cells primed at 3 DPI formed functional memory by assessing the capacity for memory T cells to produce multiple effector cytokines as well as their capacity to proliferate and expand upon rechallenge after adoptive transfer into new hosts (Fig. 5m-n).

To assess how early the memory fate is imprinted on 3 DPI transferred OT1 T cells, we sorted T cells 72 hours after adoptive transfer and performed RNA sequencing. We found that T cells were already proliferating at this time point (Supplementary Fig. 6a), and T cells transferred at 0 and 3 DPI were already transcriptionally distinct from one another and from naïve CD8 T cells (Fig. 6a). We identified 2,403 genes upregulated in 3 DPI transferred cells and 1,792 upregulated genes in 0 DPI transferred cells (Fig. 6b). Specifically, genes known to be associated with central memory cell fate, such as *Tcf7* and *Ccr7*, were upregulated in cells transferred 3 DPI, whereas genes associated with cytotoxic effector fate, such as *Ifng* and *Gzmb*, were upregulated in cells transferred 0 DPI (Fig. 6c). Geneset Enrichment Analysis further identified that cells transferred 0 DPI exhibited a highly proliferative state characterized by higher expression of genes in ribosome biogenesis, RNA transport, oxidative phosphorylation, and carbon metabolism (Supplementary Fig. 6b).

While cDC1 activation dynamics coincide precisely with this change in CD8 T cell fate, it remained possible that other cell types were contributing to this regulation. To assess whether changes in cDC1 activation state alone were sufficient to drive alternative CD8 T cell fates, we isolated cDC1s from 1.5 or 2.5 DPI and cocultured them *ex vivo* with naïve OT1 T cells such that priming would occur on 2 or 3 DPI (Fig. 6d). We found that CD8 T cells that were primed by cDC1s at 3 DPI were significantly more likely to retain CD62L expression (Fig. 6e-f). These results indicate that changes in cDC1 activation state within this narrow but critical window of time are sufficient to alter CD8 T cell fate.

Discussion

To understand how innate immune cells orchestrate an adaptive immune response, we employed high dimensional mass cytometry to generate a comprehensive map of the splenic immune response to infection. Unsupervised analysis of these data allowed for the identification of highly transient cell states across lineages. These data revealed a remarkably transient activation state for cDC1s at 2 DPI with *Lm*, characterized by peak expression of costimulatory molecules as well as MHC peptide complexes, which was also observed in the context of MCMV infection. By quantifying intrasplenic cytokines, we found that peak cDC1 activation is supported by lymphocyte-derived IFNγ. Finally, we probed the functional consequences of transient cDC1 activation. We found that T cells primed at different stages of cDC1 activation expand to different population sizes and acquire different fates. Specifically, T cells primed after peak cDC1 activation exclusively acquire memory fates. Taken together, these data suggest that transient cDC1 activation in acute infection acts as a temporal regulator of CD8 T cell fate and

contributes to the diversity of T cell fates, ensuring both a productive primary immune response as well as the development of immunological memory.

Our results also provide a unifying mechanism to contextualize several observations from prior studies. For instance, Snell and colleagues recently reported that CD8 T cells primed at 21 DPI during an established chronic viral infection preferentially differentiate into memory cells[21]. Our results show that a rapid reduction in cDC1 activation even in the first days of an acute infection are sufficient to explain this preferential memory cell differentiation. In addition, prior studies reported that CD8 T cells transferred at later times in acute viral infections exhibit delayed and reduced expansion and less Akt signaling[22,23], but the underlying mechanisms remained enigmatic due to a lack of context of the immune response dynamics across cell types. Here, we show that transient DC activation is a critical cell-extrinsic mechanism that drives diversification of CD8 T cell fates and is sufficient to explain these previous observations. In addition, we confirmed that changes in the cDC1 activation state are sufficient to drive different T cell differentiation trajectories using an *in vitro* reductionist system. Our work extends and contextualizes previous findings by comprehensively mapping the activation states of cDC1s during acute infection over time, as well as the range of activation within each timepoint. Bystander T cells and NK cells produce IFNγ early in acute infection to support host defense[24,25]. Here, we identified a new role for lymphocyte-derived IFNγ early in regulating the kinetics of cDC1 activation to support the ultimate expansion of antigen specific T cells and to regulate their balance in fates.

Elegant studies tracing the fates of single T cells have shown striking differences in expansion and fate of individual expanded clones[26,27]. Since T cell fate is imprinted within the first cell division[3,4], our study shows that the range of DC activation states throughout infection produce diverse T cell fates. Even for T cells that encounter cDC1s at the peak of their activation (2 DPI), there is a large range of highly to lowly activated cDC1s that a T cell might encounter at this time, which may thus imprint different fates. Each DC will thus express a unique combination of costimulatory molecules at varying levels as well as varying levels of MHC-peptide complexes. Future studies should build on this paradigm and trace the fates of individual T cells as a function of the activation state of their priming DCs as well as dissect how different costimulatory molecule landscapes instruct T cell differentiation.

We envision this study as a conceptual framework for studying immune responses as rapid time courses of high-dimensional single-cell data that can reveal novel mechanistic insights for how the immune system makes decisions. Our findings suggest that the structure of the immune system is a key mechanism for providing balanced protection to the host. A widely dispersed network of immune cells across tissues that undergoes waves of activation and migration utilizes time and space to provide a diverse T cell response that can both eradicate disease quickly and provide long term protection. Understanding the transient activation of DCs has broad consequences for therapeutic interventions, and we envision this work will inform future therapeutic strategies to harness these properties to tune T cell responses in infection, vaccination, cancer, or autoimmunity.

Methods

Animals

All mice were housed in an American Association for the Accreditation of Laboratory Animal Care–accredited animal facility and maintained in specific pathogen-free conditions. Animal experiments were approved and conducted in accordance with AN157618. Wild-type female C57BL/6 mice and BATF3$^{-/-}$ knockout mice between 8-10 weeks old were purchased from The Jackson Laboratory and housed at our facility. OT-3 mice were kindly provided by Stephen Schoenberger (La Jolla Institute for Immunology). IFNγ-GFP reporter mice were kindly provided by Richard Locksley (UCSF). OT-I mice were kindly provided by Lewis Lanier (UCSF). Animals were housed under standard SPF conditions with typical light/dark cycles and standard chow.

Mouse Treatments

For NK cell, T cell or IFNγ depletion experiments, mice were treated with 200 ug 1 day before infection and 1 day after infection [Anti-Thy1 (Clone 19E12 BioXcell), Anti-NK1.1 (Clone PK316 BioXcell), anti-IFNγ (Clone H22 BioXcell)]. For FTY720 blockade, mice received daily i.p. injections of FTY720 (3 mg/kg) or ethanol control beginning 2 days prior to infection.

Infectious Agents

Listeria monocytogenes strain 10403s expressing OVA (Lm-OVA) was kindly provided by Shomyseh Sanjabi (UCSF). Lm-OVA stocks frozen at −80º C were grown overnight at 37˚ C in BHI broth supplemented with 5 ug/ml erythromycin (Bio Basic, Amherst, New York). Then, overnight cultures were sub-cultured by diluting into fresh BHI broth supplemented with 5 ug/ml erythromycin and grown for 4 hours. Bacteria CFU was then quantified by measuring optical density at 600 nm. Bacteria were then diluted to 5×10^4 CFU / 100µl in sterile PBS and 100 µl was injected per mouse i.v. via the retroorbital vein. MCMV Smith strain was kindly provided by Lewis Lanier (UCSF). MCMV was passaged in BALB/c mice and a salivary gland stock was prepared as previously described[28]. Mice were infected with MCMV by i.p. injection with 1 x 10^4 pfu.

Mass Cytometry Antibodies

Primary conjugates of mass cytometry antibodies were prepared using the MaxPAR antibody conjugation kit (Fluidigm, South San Francisco, CA) according to the manufacturer's recommended protocol sourcing metals from Fluidigm (Fluidigm, South San Francisco, CA) or Trace Sciences International (Richmond Hill, Canada). Following labeling, antibodies were diluted in Candor PBS Antibody Stabilization solution (Candor Bioscience GmbH, Wangen, Germany) supplemented with 0.02% NaN_3 to between 0.1 and 0.3 mg/mL and stored long-term at 4° C. Each antibody clone and lot was titrated to optimal staining concentrations using primary mouse samples with all appropriate positive and negative controls.

Cell Preparation

All tissue preparations were performed simultaneously from each individual mouse, as previously reported [8]. After euthanasia by CO_2 inhalation, spleens were collected and homogenized in PBS + 5 mM EDTA at 4° C. All tissues were washed with PBS/EDTA and re-suspended 1:1 with PBS/EDTA and 100 mM cisplatin (Enzo Life Sciences, Farmingdale, NY) for 60 s before quenching 1:1 with PBS/EDTA + 0.5% BSA to determine viability as previously described. Cells were centrifuged at 500 x g for 5 min at 4° C and re-suspended in

PBS/EDTA/BSA at a density between 1-10 x 10^6 cells/ml. Care was taken to maintain all samples at 4° C during all phases of tissue harvest and preparation except viability staining and fixation. Suspensions were fixed for 10 min at RT using 1.6% PFA in PBS (Fisher Scientific, Hampton, New Hampshire) and frozen at -80° C.

Mass-Tag Cellular Barcoding

Mass-tag cellular barcoding was performed as previously described [29]. Briefly, 1 x 10^6 cells from each animal were barcoded with distinct combinations of stable Pd isotopes in 0.02% saponin in PBS. Samples from any given tissue from each mouse per experiment group were barcoded together. Cells were washed once with cell staining media (PBS with 0.5% BSA and 0.02% NaN_3), and once with 1X PBS, and pooled into a single FACS tube (BD Biosciences, San Jose, California). After data collection, each condition was deconvoluted using a single-cell debarcoding algorithm [29].

Mass Cytometry Staining and Measurement

Cells were resuspended in cell staining media (PBS with 0.5% BSA and 0.02% NaN_3), and antibodies against CD16 and CD32 (BioLegend, San Diego, California) were added at 20 μg/ml for 5 min at RT on a shaker to block Fc receptors. Surface marker antibodies were then added, yielding 500 uL final reaction volumes and stained for 30 min at RT on a shaker. Following staining, cells were washed 2 times with cell staining media, then permeabilized with methanol for at 10 min at 4° C. Cells were then washed twice in cell staining media to remove remaining methanol, and stained with intracellular antibodies in 500 uL for 1 hour at RT on a shaker. Cells were washed twice in cell staining media and then stained with 1 mL of 1:4000 191/193Ir DNA intercalator (Fluidigm, South San Francisco, CA) diluted in PBS with 4% PFA overnight. Cells were then washed once with cell staining media, once with PBS and once with Cell Acquisition Solution (Fluidigm, South San Francisco, CA). Care was taken to assure buffers preceding analysis were not contaminated with metals in the mass range above 100 Da. Mass cytometry samples were diluted in Cell Acquisition Solution containing bead standards (see below) to approximately 10^6 cells per mL and then analyzed on a Helios mass cytometer (Fluidigm, South San Francisco, CA) equilibrated with Cell Acquisition Solution. We analyzed 1-5 x 10^5 cells per animal per time point, consistent with generally accepted practices in the field. For adoptive transfer experiments, 1-4 x 10^6 cells per animal were analyzed.

Mass Cytometry Bead Standard Data Normalization

Data normalization was performed as previously described [7]. Briefly, just before analysis, the stained and intercalated cell pellet was resuspended in freshly prepared Cell Acquisition Solution containing the bead standard at a concentration ranging between 1 and 2 x 10^4 beads/ml. The mixture of beads and cells were filtered through a filter cap FACS tubes (BD Biosciences) before analysis. All mass cytometry files were normalized together using the mass cytometry data normalization algorithm [30], which uses the intensity values of a sliding window of these bead standards to correct for instrument fluctuations over time and between samples.

Adoptive T Cell Transfer

For adoptive transfer of pathogen specific T cells to validate the antigen specificity of transitional cells, CD8 T cells were immunomagnetically enriched from the spleens of CD45.1 or CD45.2 OT1 or OT3 TCR transgenic or from WT CD45.1 mice (for polyclonal adoptive transfer) mice with EasySep Streptavidin Negative Selection using the following biotinylated antibodies against: MHCII (AF6-120.1), CD11c (N418), Gr1 (RB6-8C5), B220 (RA3-6B2),

CD4 (GK1.5), and Ter119 (TER-119). Viable cells were quantified by counting on a hemocytometer with trypan blue staining. Cells were then resuspended in sterile PBS and transferred into naïve WT CD45.2 mice intravenously via the retroorbital vein. For most TCR transgenic adoptive transfers we transferred 5 x 10^4 cells. When sorting adoptively transferred OT-1 T cells 72 hours after transfer, we transferred 1 x 10^6 cells. For polyclonal adoptive transfers we transferred 1 x 10^6 cells. In some cases cells were also stained with CFSE.

Coculture of cDC1s and OT1 CD8 T cells

For coculture of cDC1s and OT1 CD8 T cells, mice were first infected with *Lm*-OVA. Then spleens were enriched for cDC1s using EasySep Mouse Pan-DC Enrichment Kit (StemCell Technologies, Vancouver, Canada). Samples were then stained with fluorescent antibodies staining for CD11c, MHCII, CD8, CD11b, and F480. F480-CD11c+MHCII+CD8+CD11b- cDC1s were then sorted and cocultured with immunomagnetically enriched naïve OT1 CD8 T cells. Cells were cultured in RPMI 1640 (UCSF Media Core Facility) supplemented with 10% FBS (Omega Scientific, Tarzana, California), 100 U/mL penicillin-streptomycin (Fisher Scientific, Hampton, New Hampshire), 2mM L-glutamine (Sigma-Aldrich, St. Louis, Missouri), and 50 μM β-mecaptoethanol (Thermo Fisher Scientific, Waltham, Massachusetts). No exogenous antigen or cytokines were added in order to not skew T cell fate or priming capacity. Since cDC1s were sorted at 1.5 DPI, we reasoned that priming would occur when cDC1s reached peak activation and from 2.5 DPI priming would occur after cDC1s had passed peak activation.

Flow Cytometry, Cell Sorting

Cells were stained for viability with Zombie-NIR dye. Cell surface staining was performed in cell staining media (PBS with 0.5% BSA and 0.02% NaN_3) for 30 minutes at room temperature. The following anti-mouse antibodies were used: TCRβ – APC (H57-597), CD8 – PE (53-5.8), CD62L - BV421 (MEL-14), CD45.2 – PE-Cy7 (104), CD45.1 – FITC (A20), and CD19 – APC-Cy7,. (1D3/CD19). Stained cells were analyzed with an LSR II flow cytometer (BD Biosciences). For intracellular cytokine staining, sorted T cells were restimulated with PMA and Ionomycin in the presence of brefeldin A. Cell sorting was performed on a FACSAria II (BD Biosciences).

Sample Preparation for RNA-seq

Cells were prepared as described for flow cytometry and then sorted into lysis buffer (1X Takara single-cell lysis buffer) using a FACSAria II (BD Biosciences). Tubes were then vortexed for 30 s, and flash frozen on dry ice and stored at -80°C. mRNA for each biological replicate was converted into cDNA and amplified using the Takara SMART-Seq v4 Ultra low Input RNA kit (Takara Bio). Sequencing was then performed on a NovaSeq (Illumina).

Statistical Analysis

All significance analysis was performed by unpaired two-sided student's t-test or ANOVA in R.

Unsupervised Clustering Analysis and Data Visualization

For the immune landscape across all cell types (Figure 1a-b), cell clusters were identified using the CLARA algorithm with 100 clusters as implemented in the 'cluster' package in R. For CD8 T cells only (Figure 1f), cell clusters were identified using the Phenograph algorithm with k set to 75 using the 'Cytofkit2' package in R. UMAP coordinates were identified using the 'uwot'

package in R. For cDC1 activation scores, we Z-scored proteins across all single cells in a given experiment and then summed up the Z-scores of every protein in a single cell to calculate a single score for each cell in R. For psuedotime calculations we used the PHATE dimensionality reduction algorithm with knn set to 20 and t set to 60 using the 'phateR' package in R. We then used the Phenograph algorithm with k set to 200. For Pseudotime ordering of cells we used the Slingshot algorithm specifying the starting and ending clusters using the 'slingshot' package in R. For heatmaps, we then calculated the median expression of proteins within 20 equal slices of Pseudotime.

RNA-seq Analysis

Alignment was performed using the STAR (v2.7.3a) aligner. Reads mapping to ribosomal and mitochondrial genome were removed before performing alignment. The raw read counts were estimated using HTSeq (v0.11.2). Read counts were normalized using DESeq2 to get the normalized counts. Additionally, the aligned reads were used for estimating expression of the genes using cufflinks (v2.2.1). Differential expression analysis was performed using DESeq2 with a significant differential expression analysis cutoff of P <0.05 and Fold change >= 2 or <= -2. GSEA was performed with the 'gage' package in R.

Cytokine quantification

For in vivo measurement of splenic cytokines, mouse spleens were processed in a minimal 500 uL volume of sterile PBS. Then, samples were centrifuged at 1,000 g for 10 minutes and the supernatant was removed for analysis. Samples were sent to Eve Technologies and analyzed using a multiplex cytokine array.

Antigen Specific T Cell Circulation Simulations

We sought to establish a computational framework to estimate the percentage of cells that have associated with a set of secondary lymphoid organs (SLOs) at or before a particular time point $T = t$ that would be reservoirs for priming T cells. We term this proportion P_t. We framed this problem as a multinomial sampling problem with n T cells associating with k SLOs according to a fixed probability vector p per at each discrete timepoint. Further, we specify that m SLOs ($m < k$) are associated with the infection that subject these cells to chemotaxis. Thus, we assign the set of T cells in the body, X, an SLO at t under the following sampling procedure:

$$X_t = \left(X_{t,1}, X_{t,2}, \dots, X_{t,n}\right) = Mult_k(n, p)$$

where

$$\vec{p} = \left(\overbrace{\alpha\gamma, \alpha\gamma, \dots, \alpha\gamma}^{m}, \overbrace{\gamma, \gamma, \dots, \gamma}^{k-m}\right), \sum_{i=1}^{k} p_i = 1$$

Intuitively, the probability vector represents a baseline probability of a T cell associating with any SLO (γ) but with an increased probability for the SLOs associated with chemotaxis (scaled by α). This two-variable system was constrained such that the sum of the probabilities of associating with an SLO was 1. Thus, to estimate the percentage of T cells that have associated with the m SLOs at or before timepoint $T = j$, we compute the proportion of T cells (P_t) that received the sampled value corresponding to the SLOs of interest at or before that timepoint. More precisely, our simulation reports:

$$P_t = \frac{\sum_{i=1}^{n} I\left[\left(\sum_{t=1}^{j} I[X_{t,i} \leq m]\right) \geq 1\right]}{n}$$

Where I is the indicator function. Based on our assessment of published values[18,19], we set hyperparameters k equal to 400 SLOs, m to be 4 SLOs associated with the site of infection, and the increased likelihood of associating with these sites harboring infection α to be a constant value of 8. We note that with α defined, there is a closed-form solution for γ subject to the equation noted above. The number of T cells (n) was a set to 10,000,000, an arbitrarily high value that did not impact the estimation of P_t.

Data and materials availability: Mass cytometry and RNA-seq data will be made publicly available through FlowRepository and Gene Expression Omnibus. All relevant code for figures in the paper will be available upon request.

References

1. Taniuchi, I. CD4 Helper and CD8 Cytotoxic T Cell Differentiation. *Annu. Rev. Immunol.* (2018) doi:10.1146/annurev-immunol-042617-053411.
2. Kaech, S. M., Wherry, E. J. & Ahmed, R. Effector and memory T-cell differentiation: Implications for vaccine development. *Nat. Rev. Immunol.* **2**, 251–262 (2002).
3. H, B. *et al.* Visualizing the functional diversification of CD8+ T cell responses in lymph nodes. *Immunity* **33**, 412–423 (2010).
4. Kakaradov, B. *et al.* Early transcriptional and epigenetic regulation of CD8+ T cell differentiation revealed by single-cell RNA-seq. *Nat. Immunol.* **18**, 422 (2017).
5. Kaech, S. M. & Cui, W. Transcriptional control of effector and memory CD8+ T cell differentiation. *Nat. Rev. Immunol.* **12**, 749–761 (2012).
6. Reina-Campos, M., Scharping, N. E. & Goldrath, A. W. CD8+ T cell metabolism in infection and cancer. *Nat. Rev. Immunol.* **0123456789**, (2021).
7. Spitzer, M. H. *et al.* Systemic Immunity Is Required for Effective Cancer Immunotherapy. *Cell* **168**, 487-502.e15 (2017).
8. Allen, B. M. *et al.* Systemic dysfunction and plasticity of the immune macroenvironment in cancer models. *Nat. Med.* **26**, 1125–1134 (2020).
9. Harty, J. T. & Bevan, M. J. CD8+ T cells specific for a single nonamer epitope of Listeria monocytogenes are protective in vivo. *J. Exp. Med.* **175**, 1531–1538 (1992).
10. McGregor, D. D., Koster, F. T. & Mackaness, G. B. Biological sciences: The short lived small lymphocyte as a mediator of cellular immunity. *Nature* **228**, 855–856 (1970).
11. Edelson, B. T. *et al.* CD8α+ Dendritic Cells Are an Obligate Cellular Entry Point for Productive Infection by Listeria monocytogenes. *Immunity* **35**, 236–248 (2011).
12. Theisen, D. J. *et al.* WDFY4 is required for cross-presentation in response to viral and tumor antigens. *Science (80-.).* **362**, 694–699 (2018).
13. Moon, K. R. *et al.* Visualizing structure and transitions in high-dimensional biological

data. *Nat. Biotechnol.* doi:10.1038/s41587-019-0336-3.

14. Street, K. *et al.* Slingshot: cell lineage and pseudotime inference for single-cell transcriptomics. *BMC Genomics 2018 191* **19**, 1–16 (2018).

15. Lee, S. H. *et al.* Identifying the Initiating Events of Anti- Listeria Responses Using Mice with Conditional Loss of IFN-γ Receptor Subunit 1 (IFNGR1) . *J. Immunol.* **191**, 4223–4234 (2013).

16. Bromberg, J. F., Horvath, C. M., Wen, Z., Schreiber, R. D. & Darnell, J. E. Transcriptionally active Stat1 is required for the antiproliferative effects of both interferon α and interferon γ. *Proc. Natl. Acad. Sci. U. S. A.* (1996) doi:10.1073/pnas.93.15.7673.

17. RL, R., HE, L. & RM, L. Cytokine-secreting follicular T cells shape the antibody repertoire. *Nat. Immunol.* **10**, 385–393 (2009).

18. Soderberg, K. A. *et al.* Innate control of adaptive immunity via remodeling of lymph node feed arteriole. (2005).

19. Van Heijst, J. W. J. *et al.* Recruitment of antigen-specific cd8+ t cells in response to infection is markedly efficient. *Science (80-.).* **325**, 1265–1269 (2009).

20. Enouz, S., Carrié, L., Merkler, D., Bevan, M. J. & Zehn, D. Autoreactive T cells bypass negative selection and respond to self-antigen stimulation during infection. *J. Exp. Med.* **209**, 1769–1779 (2012).

21. Snell, L. M. *et al.* CD8+ T Cell Priming in Established Chronic Viral Infection Preferentially Directs Differentiation of Memory-like Cells for Sustained Immunity. *Immunity* **49**, 678-694.e5 (2018).

22. D'Souza, W. N. & Hedrick, S. M. Cutting Edge: Latecomer CD8 T Cells Are Imprinted with a Unique Differentiation Program. *J. Immunol.* **177**, 777–781 (2006).

23. Quigley, M., Huang, X. & Yang, Y. Extent of Stimulation Controls the Formation of Memory CD8 T Cells. *J. Immunol.* (2007) doi:10.4049/jimmunol.179.9.5768.

24. Berg, R. E., Crossley, E., Murray, S. & Forman, J. Memory CD8+ T Cells Provide Innate Immune Protection against Listeria monocytogenes in the Absence of Cognate Antigen. *J. Exp. Med.* **198**, 1583–1593 (2003).

25. Soudja, S. M., Ruiz, A. L., Marie, J. C. & Lauvau, G. Inflammatory monocytes activate memory CD8+ T and innate NK lymphocytes independent of cognate antigen during microbial pathogen invasion. *Immunity* **37**, 549 (2012).

26. Buchholz, V. R. *et al.* Disparate individual fates compose robust CD8+ T cell immunity. *Science (80-.).* (2013) doi:10.1126/science.1235454.

27. Gerlach, C. *et al.* Heterogeneous differentiation patterns of individual CD8+ T cells. *Science (80-.).* **340**, 635–639 (2013).

28. Bubić, I. *et al.* Gain of Virulence Caused by Loss of a Gene in Murine Cytomegalovirus. *J. Virol.* **78**, 7536–7544 (2004).

29. Zunder, E. R. *et al.* Palladium-based Mass-Tag Cell Barcoding with a Doublet-Filtering Scheme and Single Cell Deconvolution Algorithm. *Nat. Protoc.* **10**, 316–333 (2015).

30. Finck, R. *et al.* Normalization of mass cytometry data with bead standards. *Cytom. Part A*

83 A, 483–494 (2013).

Acknowledgments:

Funding:

Funding support from NIH grant DP5OD023056, the Chan Zuckerberg Biohub, the UCSF Program for Breakthrough Biomedical Research, and AACR NextGen Transformative Cancer Research Grant to MHS, and NIH grant S10OD018040, which enabled procurement of the CyTOF mass cytometer used in this study. KJHG is supported by a Stanford Propel Scholar award and a CRI Irvington Fellowship. CAL is supported by a Stanford Science Fellowship and Parker Scholar award. TLHO is supported by the Carlsberg Foundation.

Figures:

Schematics were created with BioRender.com

Author contributions:

Conceptualization: KJHG, MHS

Methodology: KJHG, RD, CAL, TLHO

Investigation: KJHG, RD, NWC, JLY

Visualization: KJHG, RD, CAL, TLHO

Funding acquisition: MHS

Project administration: KJHG, MHS

Supervision: KJHG, MHS

Writing – original draft: KJHG, MHS

Writing – review & editing: KJHG, RD, CAL, NWC, MHS

Competing interests: MHS is a shareholder and board member of Teiko Bio; received consultant fees from Five Prime Therapeutics, Earli, Ono Pharmaceutical, and January; and received research funding from Roche/Genentech, Pfizer, Valitor, and Bristol-Myers Squibb.

Figures

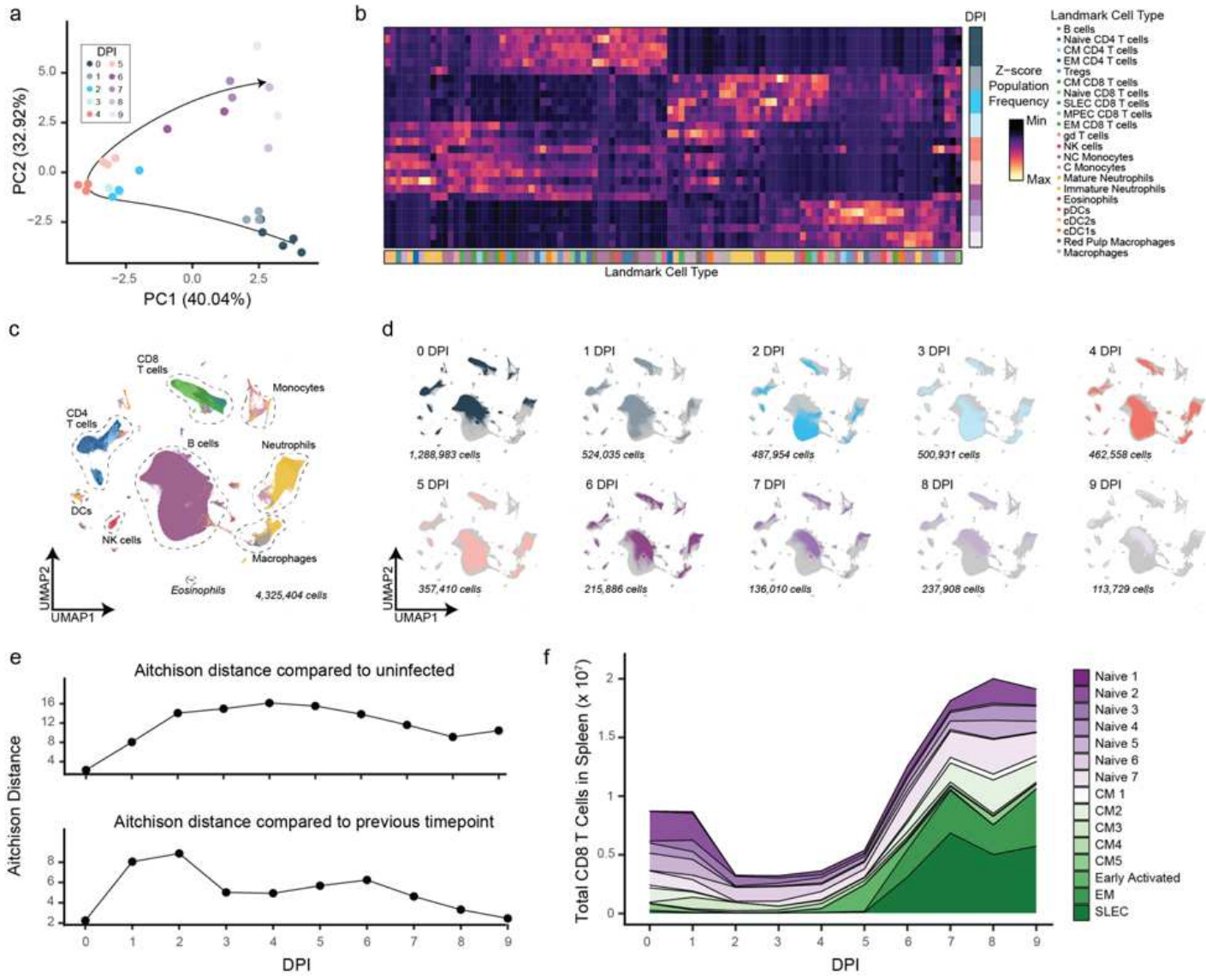

Figure 1

Immune landscape shifts during acute infection. (a) Principal component analysis of mouse spleen population frequencies throughout infection measured by mass cytometry. Populations were identified by unsupervised clustering. (n = 5 independent animals for 0 DPI, n = 3 1-5 DPI, n = 2 6-9 DPI) (b) Normalized frequencies as a percent of total cells for all unsupervised clusters in each mouse. (c) UMAP dimensionality reduction of all cells measured across samples colored by major landmark population. (d) Cells from each timepoint superimposed on the total immune landscape. (e) Quantification of compositional changes throughout infection by Aitchison distance. Splenic landscapes from each timepoint are compared to either uninfected mice or the preceding timepoint. (f) Total frequencies of splenic CD8 T cell subsets identified by unsupervised clustering.

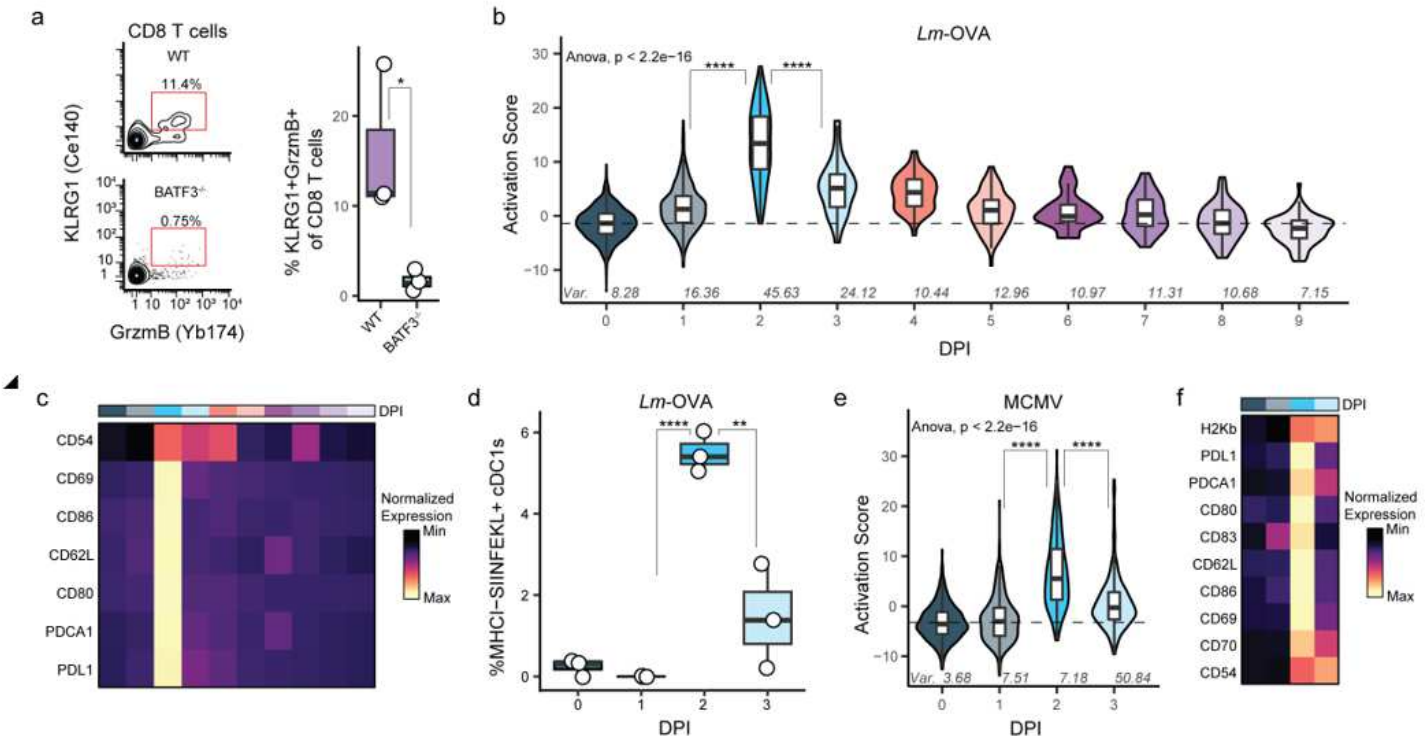

Figure 2

Transient cDC1 activation during acute infection. (a) Representative scatter plots and quantification of splenic cytotoxic effector CD8 T cells at 7 DPI with Lm-OVA in wild type or BATF3-/- mice. (n = 3 independent animals per genotypes) (b) Composite activation score (CD80, CD86, CD83, CD54, CD69, PDCA1, CD62L, and PDL1) in single cDC1s plotted throughout infection with Lm-OVA. Variance at each timepoint quantified in italics. (n = 5 independent animals for 1 DPI, n = 3 1-5 DPI, n = 2 6-9 DPI) (c) Normalized expression of all molecules used to calculate activation score during Lm-OVA infection. (d) Percent of cDC1s expressing high levels of MHCI-SIINFEKL complexes during early infection with Lm-OVA. (n = 3 independent animals per timepoint) (e) Composite activation score (CD80, CD86, CD83, CD54, CD69, PDCA1, CD62L, H2-Kb, CD70, MHC II and PDL1) in single cDC1s plotted throughout infection with MCMV. Variance at each timepoint quantified in italics. (n = 5 independent animals for 0 DPI, n = 3 independent animals for 1-2 DPI, n = 4 independent animals for 3 DPI) (f) Normalized expression of all molecules used to calculate activation score during MCMV infection. For all box plots, *P<0.05, **P<0.01, ***P<0.001, and ****P<0.0001 by two sided t-test with Benjamini-Hochberg correction. Box plots: center line, median; box limits, upper and lower quartiles; whiskers, 1.58x interquartile range/sqrt (n).

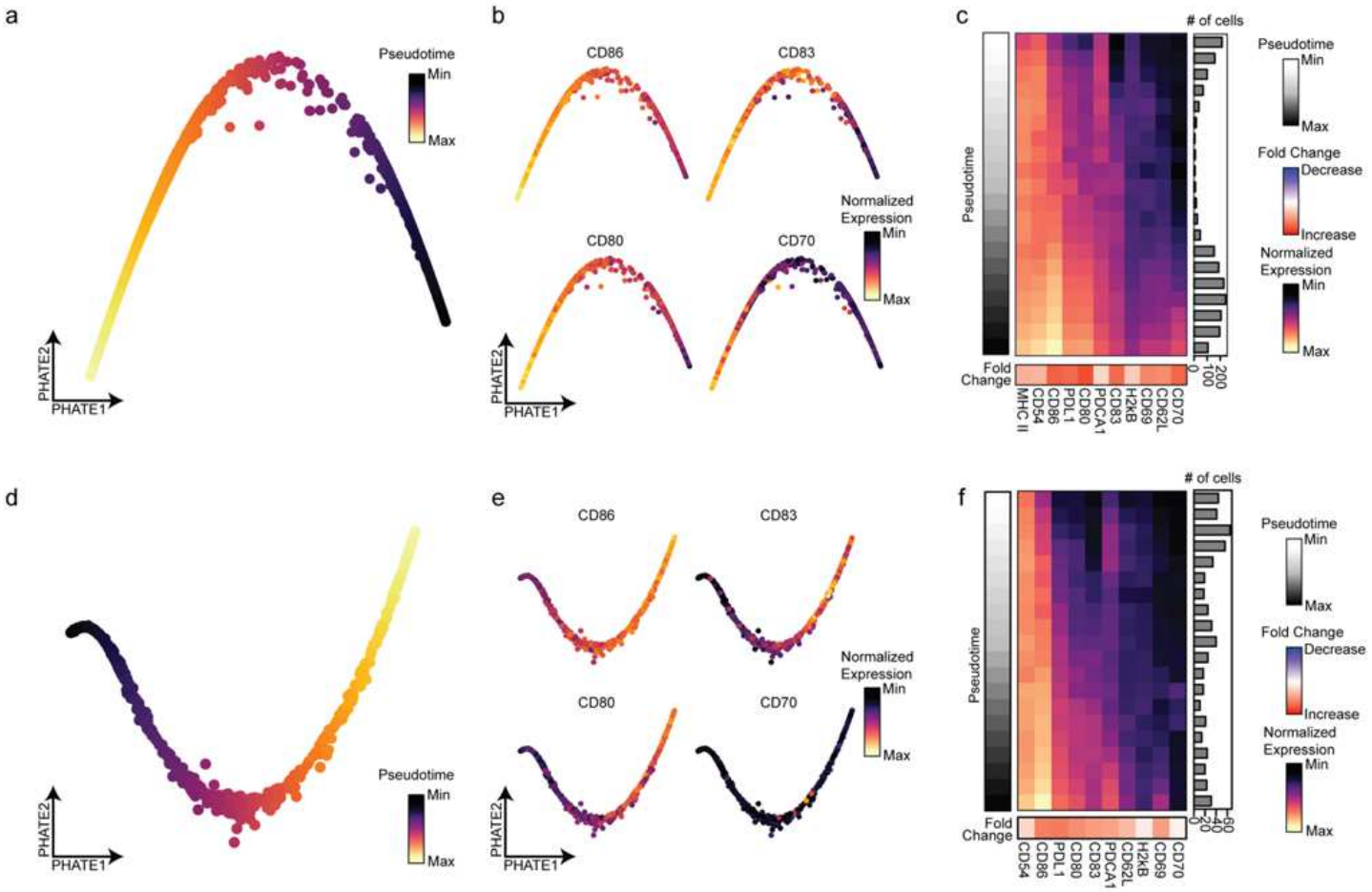

Figure 3

Coordinated activation trajectory of cDC1s during acute infection (a) PHATE dimensionality reduction of cDC1s at 2 DPI with Lm-OVA colored by Pseudotime. (n = 4 independent animals) (b) Expression of key costimulatory and activation markers in cDC1s at 2 DPI with Lm-OVA. (c) Normalized protein expression in cDC1 at 2 DPI with Lm-OVA grouped into 20 bins based on pseudotime. Fold change in expression from minimum to maximum Pseudotime plotted on the x-axis and number of cells in each Pseudotime bin plotted on the y-axis. (d) PHATE dimensionality reduction of cDC1s at 2 DPI with MCMV colored by Pseudotime. (e) Expression of key costimulatory and activation markers in cDC1s at 2 DPI with MCMV. (n = 4 independent animals) (g) Normalized protein expression in cDC1 at 2 DPI with MCMV grouped into 20 bins based on pseudotime. Fold change in expression from minimum to maximum Pseudotime plotted on the x-axis and number of cells in each Pseudotime bin plotted on the y-axis.

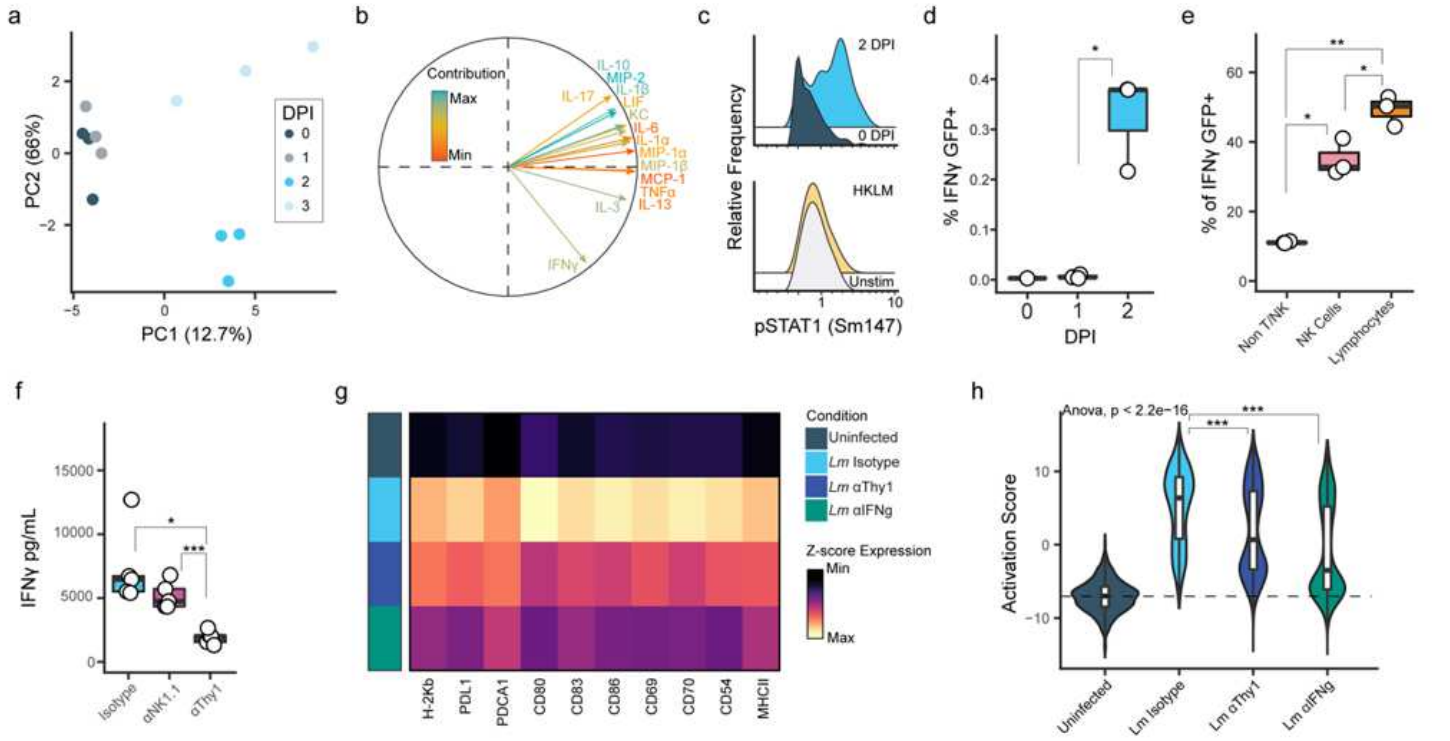

Figure 4

T cell derived IFNγ supports peak cDC1 activation. (a) Principal component analysis of mouse spleen cytokines during early Lm-OVA infection. (n = 3 independent animals per timepoint) (b) Vector plot of top 15 cytokines contributing to PC1 and PC2 colored by contribution. (c) pSTAT1 expression from splenic cDC1s at 2 DPI with Lm-OVA or uninfected mice and after 15 minutes of incubation with HKLM ex vivo or unstimulated. (d) Quantification of GFP+ cells in the spleen of IFNγ-GFP reporter mice after infection with Lm-OVA. (n = 2 independent animals for 0 DPI, n = 3 independent animals for 1-2 DPI) (e) Quantification of the cellular identity of GFP+ cells at 2 DPI with Lm-OVA. (f) Quantification of splenic IFNγ at 2 DPI with Lm-OVA after antibody depletion of NK cells or Thy1+ lymphocytes. (n = 4 independent animals for Isotype treated and n = 5 independent animals for Uninfected, α-Thy1, α-IFNγ) (g) Normalized mean expression of key proteins in splenic cDC1s at 2 DPI with Lm-OVA following depletion of T cells or IFNγ. (h) Composite activation score (CD80, CD86, CD83, CD54, CD69, PDCA1, CD62L, H2-Kb, CD70, MHC II and PDL1) in splenic cDC1s at 2 DPI with Lm-OVA following depletion of lymphocytes or IFNγ. For all box plots, *P<0.05, **P<0.01, and ***P<0.001 by two sided t-test with Benjamini-Hochberg correction. Box plots: center line, median; box limits, upper and lower quartiles; whiskers, 1.58x interquartile range/sqrt (n).

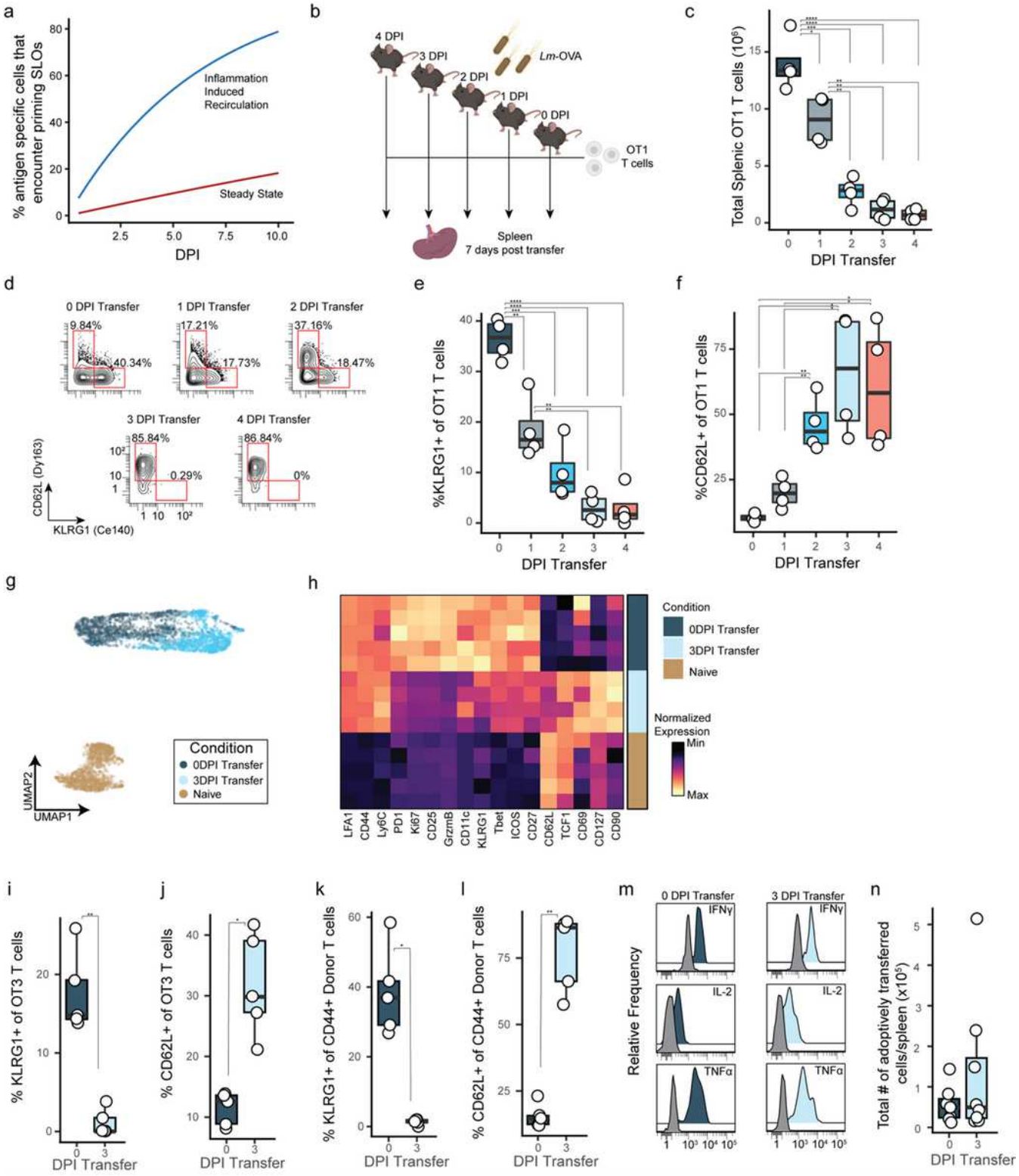

Figure 5

CD8 T cells primed after peak cDC1 activation acquire memory fates. (a) Simulation depicting the cumulative proportion of antigen specific T cells that pass through a SLO capable of priming. (b) Schematic for experimental testing of late arriving T cell differentiation capacities in which OT1 CD8 T cells are adoptively transferred into mice 0-4 DPI with Lm-OVA and then harvested after 7 days. (c) Quantification of splenic OT1 CD8 T cell expansion by DPI of adoptive transfer in Lm-OVA. (n = 4

independent animals per condition) (d) Representative scatter plots of CD8 T cells after 7 days of differentiation from experiment depicted in (b). Quantification of splenic KLRG1+ SLEC (e) or CD62L+ central memory cells (f) OT1 CD8 T cells by DPI of adoptive transfer in Lm-OVA. (g) UMAP dimensionality reduction of equal numbers of OT1 CD8 T cells transferred at 0 or 3 DPI and then harvested from spleens 7 days after transfer. (n = 5 independent animals for 0DPI transfer and Naïve, n = 4 independent animals for 3DPI transfer) (h) Normalized median expression of key T cell differentiation and activation markers 7 days after transfer in 0DPI, 3DPI, or naïve OT1 CD8 T cells. Quantification of splenic KLRG1+ SLEC (i) or CD62L+ central memory (j) OT3 CD8 T cells by DPI of adoptive transfer in Lm-OVA (n = 5 independent animals per condition). Quantification of splenic KLRG1+ SLEC (k) or splenic CD62L+ central memory (l) polyclonal CD8 T cells by DPI of adoptive transfer in MCMV (n = 5 independent animals per condition). (m) Representative histograms of 0 or 3 DPI Lm-OVA transferred memory OT1 CD8 T cells restimulated with PMA & Ionomycin 40 DPI. (n) Quantification of 0 or 3 DPI Lm-OVA memory OT1 T cells retransferred into new hosts at 40 DPI and rechallenged. Cell counts are 7 DPI rechallenge. (n = 7 independent animals for 0DPI transfer, n = 8 independent animals for 3DPI transfer) For all box plots, *P<0.05, **P<0.01, ***P<0.001, and ****P<0.0001 by two sided t-test with Benjamini-Hochberg correction. Box plots: center line, median; box limits, upper and lower quartiles; whiskers, 1.58x interquartile range/sqrt (n).

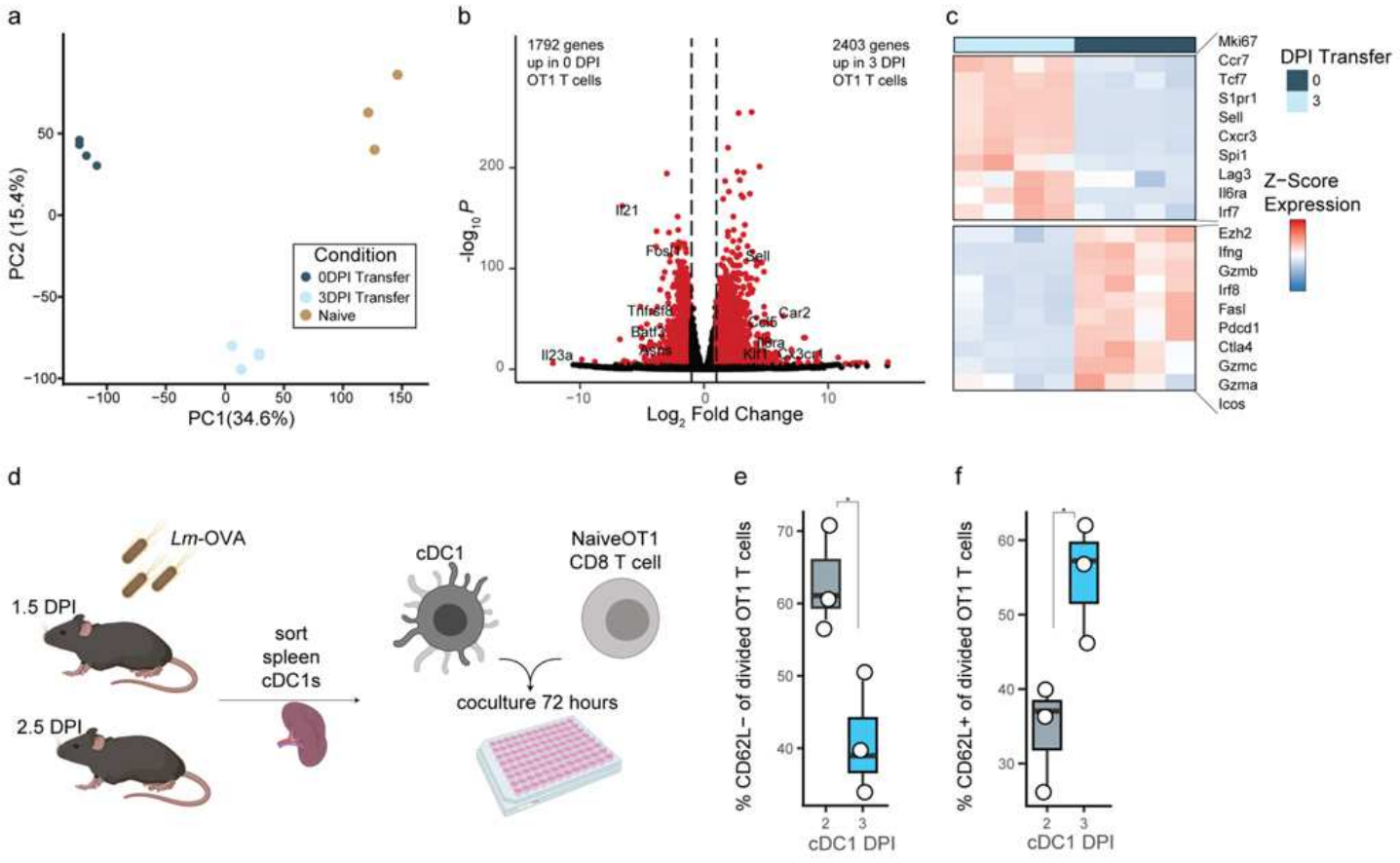

Figure 6

Memory fate in T cells primed after cDC1 peak activation is imprinted by¬ cDC1s. (a) Principal component analysis of RNA-seq of naïve and 0 or 3 DPI Lm¬-OVA primed OT1 CD8 T cells 72 hours after transfer. (n = 3 independent animals for Naïve, n = 4 independent animals for 0DPI and 3DPI transfer) (b) Volcano plot of differentially expressed genes between 0DPI and 3DPI OT1 CD8 T cells 72 hours after transfer (fold change >2; P-value <10e-6). (c) Normalized expression of differentially expressed genes known to be involved in memory or effector fates. (d) Schematic for experimental testing of T cell priming capacity of cDC1s from different timepoints of infection. Splenic cDC1s are sorted from mice at 1.5 or 2.5 DPI with Lm-OVA and then incubated with naïve OT1 CD8 T cells for 3 days such that priming occurs during peak cDC1 activation or after peak cDC1 activation (2 or 3 DPI). Quantification of CD62L- effector (e) or CD62L+ memory (f) OT1 T cells primed ex vivo by cDC1s from 2 or 3 DPI Lm-OVA. (n = 3 independent replicates per condition of cDC1s pooled from 3 different mice per condition). For all box plots, *P<0.05 by two sided t-test. Box plots: center line, median; box limits, upper and lower quartiles; whiskers, 1.58x interquartile range/sqrt (n).

Supplementary Files

This is a list of supplementary files associated with this preprint. Click to download.

- HiamGalvezSupplementaryMaterials.pdf